The Astrophysical Journal Letters, 764:L23 (5pp), 2013 February 20 doi:10.1088/2041-8205/764/2/L23

A DOUBLE-PEAKED OUTBURST OF A 0535+26 OBSERVED WITH *INTEGRAL*, *RXTE*, AND *SUZAKU*

I. Caballero[1], K. Pottschmidt[2,3], D. M. Marcu[2,3], L. Barragan[4], C. Ferrigno[5], D. Klochkov[6], J. A. Zurita Heras[7], S. Suchy[6], J. Wilms[4], P. Kretschmar[8], A. Santangelo[6], I. Kreykenbohm[4], F. Fürst[9], R. Rothschild[10], R. Staubert[6], M. H. Finger[11], A. Camero-Arranz[12], K. Makishima[13,14], T. Enoto[14], W. Iwakiri[15], and Y. Terada[15]
[1] Laboratoire AIM, CEA/IRFU, CNRS/INSU, Université Paris Diderot, CEA DSM/IRFU/SAp, F-91191 Gif-sur-Yvette, France; isabel.caballero@cea.fr
[2] Center for Space Science and Technology, University of Maryland Baltimore County, 1000 Hilltop Circle, Baltimore, MD 21250, USA
[3] CRESST, NASA Goddard Space Flight Center, Astrophysics Science Division, Code 661, Greenbelt, MD 20771, USA
[4] Dr. Karl Remeis-Sternwarte and ECAP, FAU Erlangen-Nuremberg, Sternwartstr. 7, D-96049 Bamberg, Germany
[5] ISDC Data Centre for Astrophysics, University of Geneva, Chemin d'Ecogia 16, CH-1290 Versoix, Switzerland
[6] Institut für Astronomie und Astrophysik, Sand 1, D-72076 Tübingen, Germany
[7] François Arago Centre, APC (UMR 7164 Université Paris Diderot, CNRS/IN2P3, CEA/DSM, Observatoire de Paris), 13 rue Watt, F-75205 Paris Cedex 13, France
[8] European Space Astronomy Centre (ESA/ESAC), Science Operations Department, Villanueva de la Cañada, E-28080 Madrid, Spain
[9] Space Radiation Lab, California Institute of Technology, MC 290-17 Cahill, 1200 E. California Blvd., Pasadena, CA 91125, USA
[10] Center for Astrophysics and Space Science, UCSD, La Jolla, CA 92093, USA
[11] National Space Science and Technology Center, 320 Sparkman Drive NW, Huntsville, AL 35805, USA
[12] Institut de Ciències de l'Espai (IEEC-CSIC), Campus UAB, Fac. de Ciències, Torre C5, parell, 2a planta, E-08193 Barcelona, Spain
[13] Department of Physics, The University of Tokyo, 7-3-1 Hongo, Bunkyo, Tokyo 113-0033, Japan
[14] Cosmic Radiation Laboratory, RIKEN, 2-1, Hirosawa, Wako City, Saitama 351-0198, Japan
[15] Graduate School of Science and Engineering, Saitama University, 255 Shimo-Okubo, Sakura, Saitama 338-8570, Japan
Received 2012 November 23; accepted 2013 January 18; published 2013 February 4

ABSTRACT

The Be/X-ray binary A 0535+26 showed a normal (type I) outburst in 2009 August. It is the fourth in a series of normal outbursts associated with the periastron, but is unusual because it presented a double-peaked light curve. The two peaks reached a flux of ∼450 mCrab in the 15–50 keV range. We present results of the timing and spectral analysis of *INTEGRAL*, *RXTE*, and *Suzaku* observations of the outburst. The energy-dependent pulse profiles and their evolution during the outburst are studied. No significant differences with respect to other normal outbursts are observed. The centroid energy of the fundamental cyclotron line shows no significant variation during the outburst. A spectral hardening with increasing luminosity is observed. We conclude that the source is accreting in the sub-critical regime. We discuss possible explanations for the double-peaked outburst.

Key words: pulsars: individual (A 0535+26) – stars: magnetic field – X-rays: binaries – X-rays: stars

Online-only material: color figure

1. INTRODUCTION

The Be/X-ray binary A 0535+26 was discovered during a giant outburst with *Ariel V* (Rosenberg et al. 1975). At a distance of $d \sim 2$ kpc, it consists of the B0 IIIe optical companion HDE 245770 (Steele et al. 1998) and a pulsating neutron star of spin period $P_{\rm spin} \sim 103$ s, in an eccentric orbit ($e = 0.47$) with a period of $P_{\rm orb} = 111.1$ days (Finger et al. 2006). The system presents different luminosity states associated with the activity of the Be star: quiescence, with X-ray luminosities $L_{\rm X} \lesssim 10^{36}\,{\rm erg\,s^{-1}}$ (Rothschild et al. 2013), normal (type I) outbursts, with luminosities $L_{\rm X} \sim 10^{36-37}\,{\rm erg\,s^{-1}}$, and giant (type II) outbursts that can reach luminosities $L_{\rm X} > 10^{37}\,{\rm erg\,s^{-1}}$ (see, e.g., Finger et al. 1996). A 0535+26 presents two cyclotron resonance scattering features (or cyclotron lines) in its X-ray spectrum at ∼46 and ∼100 keV (see, e.g., Caballero et al. 2007 and references therein). Cyclotron lines are caused by resonant scattering of photons off electrons in the quantized Landau levels, and the cyclotron line energy is proportional to the magnetic field strength, $E_{\rm cyc} = \hbar eB/m_e c = 11.6\,{\rm keV}\cdot B/10^{12}\,{\rm G}$ (e.g., Schönherr et al. 2007).

Some accreting X-ray pulsars present a negative correlation between the cyclotron line centroid energy and the X-ray luminosity (e.g., 4U 0115+64,[16] V 0332+53; see Nakajima et al. 2006; Tsygankov et al. 2006; Mowlavi et al. 2006). Other sources, like Her X-1, GX 304−1, and Swift J1626.6−5156 show the opposite trend (Staubert et al. 2007; Klochkov et al. 2012; DeCesar et al. 2013). As discussed by Becker et al. (2012), this bimodality is probably due to two different accretion regimes depending on the critical luminosity $L_{\rm crit}$. For sources with $L_{\rm X} > L_{\rm crit}$ (*supercritical* sources), a radiative shock decelerates the infalling matter, with the height of the emission region increasing with increasing mass accretion rate, explaining the negative correlation between the cyclotron line energy and the X-ray luminosity. On the other hand, for sources with $L_{\rm X} < L_{\rm crit}$ (*subcritical* sources), Coulomb interactions stop the infalling matter, and the height of the emission region decreases with increasing accretion rate, explaining the positive correlation observed (further details in Becker et al. 2012, see also Basko & Sunyaev 1976; Staubert et al. 2007). Contrary to these sources, for A 0535+26, no significant correlation between the cyclotron line energy and the X-ray luminosity has been observed (Terada et al. 2006; Caballero et al. 2007), with the exception of a flaring episode during the onset of a normal outburst observed in 2005 during which the cyclotron line energy significantly increased (see Caballero et al. 2008; Postnov et al. 2008, for details). These results refer to pulse phase-averaged spectroscopy; see, however, Klochkov et al. (2011) for pulse-to-pulse analysis in which a positive correlation between the flux and the cyclotron line energy was observed.

[16] See, however, Müller et al. (2012b), where it is shown that for 4U 0115+64, the presence of a correlation depends on the model for the continuum.

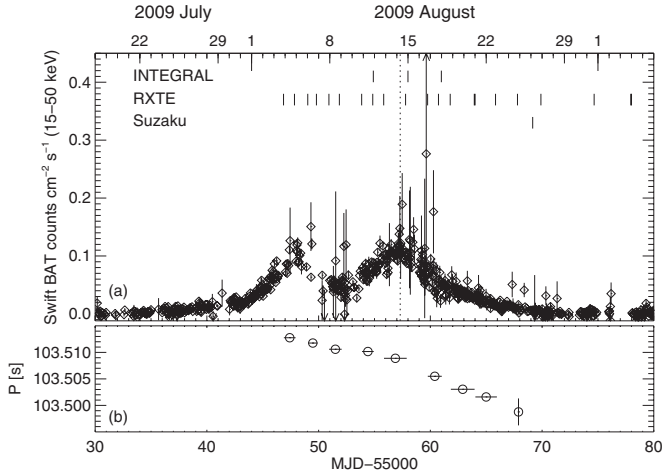

Figure 1. (a) *Swift*/BAT orbital light curve (15–50 keV) of the A 0535+26 double-peaked outburst. The tick marks indicate the times of the *INTEGRAL*, *RXTE*, and *Suzaku* observations presented in this work. The vertical dotted line shows the time of periastron. (b) Pulse period evolution derived from the *RXTE* observations.

A 0535+26 showed a giant outburst and a series of normal ones in 2009, all of them associated with the periastron passage of the neutron star (Caballero et al. 2009). The giant outburst reached a flux of $F_{(15-50)\,\mathrm{keV}} = (1.17 \pm 0.04)$ counts s^{-1} cm^{-2} ($\sim$5.3 Crab[17]) at MJD 55179.0 and lasted about 40 days. In this work, we focus on a double-peaked outburst that preceded the giant one. We present *INTEGRAL*, *RXTE*, and *Suzaku* observations of the outburst. The *Swift*/Burst Alert Telescope (BAT) light curve of the outburst and the times of the observations are shown in Figure 1(a). The first peak of the outburst reached a flux of $F_{(15-50)\,\mathrm{keV}} = (0.100 \pm 0.004)$ counts s^{-1} cm^{-2} ($\sim$455 mCrab[17]) at MJD 55048.0, which decreased to $F_{(15-50)\,\mathrm{keV}} = (0.047 \pm 0.002)$ counts s^{-1} cm^{-2} ($\sim$214 mCrab) at MJD 55051.0 and rose again, reaching $F_{(15-50)\,\mathrm{keV}} = (0.104 \pm 0.005)$ counts s^{-1} cm^{-2} ($\sim$471 mCrab) at MJD 55058.0 around periastron. The observations are described in Section 2. The results of the timing and spectral analyses are presented in Section 3, and the results are discussed in Section 4.

2. OBSERVATIONS AND DATA ANALYSIS

We made use of *INTEGRAL* data collected with the gamma-ray spectrometer SPectrometer on *INTEGRAL* (SPI, 20 keV–8 MeV; Vedrenne et al. 2003), the imager IBIS (15 keV–10 MeV; Ubertini et al. 2003), and the X-ray monitor JEM-X (3–35 keV; Lund et al. 2003). Three pointed observations were performed around the second peak of the outburst (MJD start 55054.89, 55057.99, and 55060.99). The JEM-X and SPI data analyses were performed using the standard analysis package OSA v9. For IBIS, we used OSA v10, which contains a new energy calibration for ISGRI.

RXTE (Bradt et al. 1993) performed regular pointed observations of A 0535+26 during the outburst between MJD 55046.86 and 55078.00 (Proposal ID P94323). We used data from the Proportional Counter Array (PCA, 2–60keV; Jahoda et al. 1996) and the High Energy X-ray Timing Experiment (HEXTE, 20–200 keV; Rothschild et al. 1998). The *RXTE* data were analyzed using HEASOFT v6.7. We restricted the PCA spectral analysis to energies above 5 keV due to a feature around 5 keV caused by instrumental Xe L edges (Rothschild et al. 2006).

Suzaku performed one observation of A 0535+26 during the decay of the outburst (MJD start 55067.96, ObsID 404054010). We used data from the two main instruments, the X-ray Imaging Spectrometer (XIS; Koyama et al. 2007) and the Hard X-ray Detector (HXD; Takahashi et al. 2007). The data analysis was performed using HEASOFT v6.12 and CALDB versions 20110913 for HXD, 20120209 for XIS, and 20110630 for XRT. We used XIS data between 0.5 and 10 keV for XIS 1, and data between 0.7 and 10 keV for XIS 0, 3. XIS data were binned as in Nowak et al. (2011). Because of the XIS calibration uncertainties, especially around the Si K edge at $\sim$1.8 keV, a systematic error of 1% was assumed for the XIS data. The spectral analysis was performed with *XSPEC* v12.7.0.

3. RESULTS

3.1. Timing Analysis

We studied the pulse period evolution using the phase-connection technique described by Staubert et al. (2009). We extracted PCA light curves with 15.6 ms resolution in the 3.3–42.8 keV range. Barycentric and orbital corrections were applied to the light curves, using the ephemeris from Finger et al. (2006). The evolution of the pulse period is shown in Figure 1(b). A decrease in the pulse period along the outburst is observed. A linear fit can be used to describe the pulse period evolution between MJD 55046.89 and 55057.88, during the two main peaks of the outburst. We find a pulse period of $P = 103.51263 \pm 0.00004$ s and spin-up of $\dot{P} = (-0.459 \pm 0.005) \times 10^{-8}$ s s^{-1} at MJD 55047.4. The pulse period during the decay of the outburst (MJD $>$ 55057.88) can also be described with a linear fit. We obtain a spin period of $P = 103.50886 \pm 0.00001$ s for MJD 55056.87 and a spin-up of $\dot{P} = (-1.104 \pm 0.002) \times 10^{-8}$ s s^{-1}.

Making use of these pulse period values to fold the light curves, we studied the evolution of the energy-dependent pulse profiles using all of the *RXTE* pointed observations. During the two main peaks of the outburst, the pulse profiles are remarkably stable, showing a complex structure at low energies, and becoming simpler at higher energies. The shape of the pulse profiles at low energies slightly varies towards the decay of the outburst. As an example, the pulse profiles for one observation during the first peak of the outburst and one observation during the decay are shown in Figure 2.

3.2. Spectral Analysis

We studied the broadband spectral continuum and its evolution during the outburst with *RXTE*, *INTEGRAL*, and *Suzaku*. It can be described by a power law with an exponential cutoff, typical for accreting X-ray binaries (see, e.g., White et al. 1983). We used the *XSPEC* model `cutoffpl`, given by $F(E) \propto E^{-\Gamma} e^{-E/E_{\mathrm{fold}}}$, where Γ and E_{fold} are the photon index and folding energy, respectively.

The *Suzaku* spectrum was modeled including an additional blackbody component, photoelectric absorption, and a Gaussian line in emission to account for the Fe Kα line. The presence of the Fe Kα line is marginal, and the line energy and width have been fixed to 6.4 and 0.5 keV, respectively. Its inclusion in the model yields an improvement in the χ^2_{red}/dof from 1.43/581 to 1.37/580. The equivalent width of the line is EW (Fe Kα) = 70 $\pm$ 2 eV. The inclusion of the blackbody component in the model leads to an improvement in the

[17] Fluxes derived from the daily *Swift*/BAT transient monitor results provided by the *Swift*/BAT team; $\sim$0.22 counts s^{-1} cm^{-2} correspond to 1 Crab.

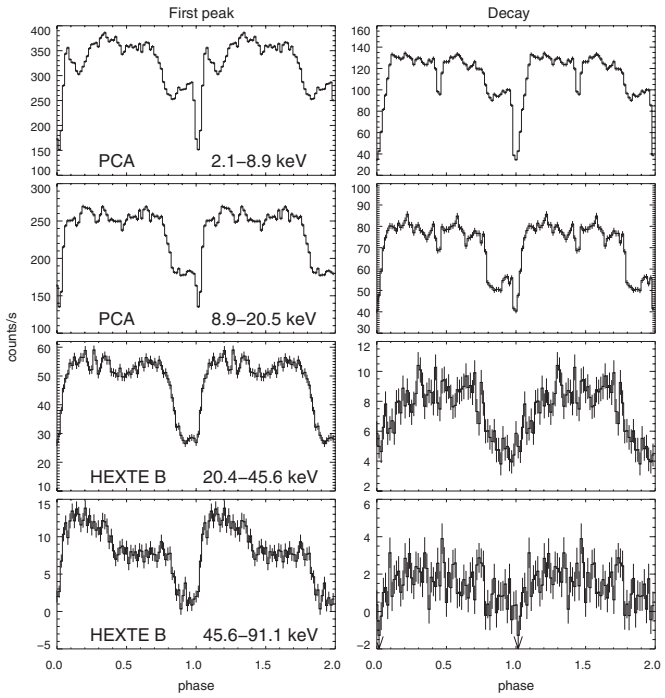

Figure 2. *RXTE* PCA and HEXTE energy-dependent pulse profiles for one observation around the first peak (left, MJD 55047.86, ObsID 94323-02-03-01) and one observation during the decay of the outburst (right, MJD 55065.84, ObsID 94323-03-02-01). The energy ranges are indicated in the left panels, and are the same for both observations. The PCA count rate is given in counts s^{-1} PCU^{-1}. Two pulse cycles are shown for clarity.

χ^2_{red}/dof from 3.01/582 to 1.37/580, giving an *F*-test significance >99.99%. The best-fit value of the blackbody temperature is $k_BT = 1.26^{+0.05}_{-0.04}$ keV. Setting the cross-sections and the abundances to those from Verner et al. (1996) and Wilms et al. (2000), respectively, we obtained an absorption column of $N_H = 0.70 \pm 0.03 \times 10^{22}$ atoms cm^{-2}.

To model the *RXTE* spectra, we added a Gaussian emission line to account for residuals present in the 5–7 keV range. The energy of the line was left free, and the width of the line was frozen to the best-fit value in each observation. The line energy obtained for the different observations varies between 5.0 and 6.6 keV, consistent with the instrumental Xe L edge at ∼5 keV and the 6.4 keV Fe Kα line. It was not possible to model the two components independently.

In the *INTEGRAL*, *Suzaku*, and most of the *RXTE* observations, a significant absorption-like feature is present in the residuals at $E \sim 46$ keV that we model using a Gaussian optical depth profile $\tau(E) = \tau e^{-(E-E_{cyc})^2/(2\sigma^2)}$, which modifies the continuum as $F'(E) = F(E)e^{-\tau(E)}$. As an example, the broadband spectrum of the second *INTEGRAL* observation is shown in Figure 3 (left). In this case, the inclusion of a cyclotron line in the model yields an improvement in the χ^2_{red}/dof from 8.8/132 to 0.88/129. The *Suzaku* broadband spectrum is shown in Figure 3 (right). The inclusion of a cyclotron line in this case improves the χ^2_{red}/dof from 1.73/583 to 1.37/580.

We studied the evolution of the cyclotron line centroid energy, photon index, and folding energy as a function of time and X-ray luminosity. To study the evolution of the different spectral parameters, we selected the first 16 *RXTE* observations (MJD 55046.86–55065.84), which are the ones where the cyclotron line was significantly detected. The first harmonic line at $E \sim 100$ keV, observed in brighter outbursts of the source (e.g., Caballero et al. 2007), is not significantly detected in the observations presented here. The results are shown in Figure 4. No dependency of the cyclotron line energy with the X-ray luminosity is found. We checked that the choice of continuum model does not affect the line parameters by fitting the continuum using an exponentially cutoff power law, a Fermi–Dirac cutoff power law (Tanaka 1986), and a power law with an exponential cutoff starting at a cutoff energy (the `highecut` model of *XSPEC*). In all three cases, the line parameters remain the same within their error bars (see also Caballero 2009). A linear fit to the E_{cyc} versus L_X values gives a slope of (-3 ± 3) keV/10^{37}erg s^{-1} using *RXTE* data only, and (-0.9 ± 2.0) keV/10^{37}erg s^{-1} using *RXTE*, *INTEGRAL*, and *Suzaku* data. We included intercalibration constants for the different instruments in the separate *RXTE*, *INTEGRAL*, and *Suzaku* spectral analyses. For the *Suzaku* analysis, we fixed the constant to 1 for XIS 0 and allowed the others to vary. In the case of the Gadolinium Silicate detector (GSO) detector of

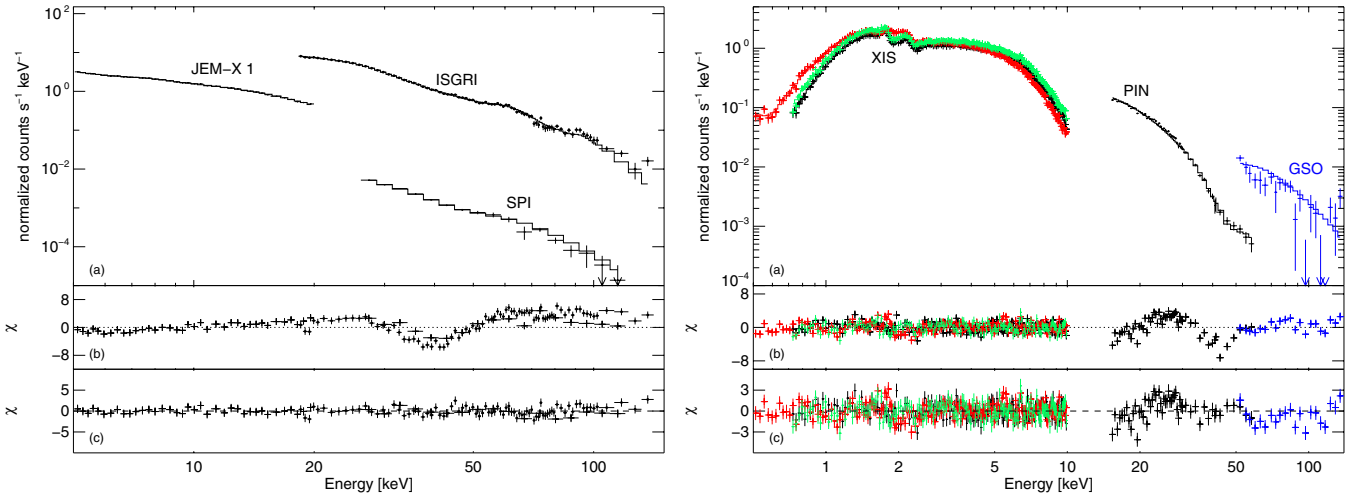

Figure 3. Left: *INTEGRAL* spectrum of A 0535+26 (MJD 55057.99). (a) Data and best-fit model. (b) Residuals of a fit including no absorption lines in the model. (c) Residuals of a fit including one line at ∼46 keV in the model. The filled circles represent the ISGRI data. The average flux during the observation $F_{20-100\,keV} \sim 5.0 \times 10^{-9}$ erg cm^{-2} s^{-1}. Right: *Suzaku* spectrum of A 0535+26 (MJD 55067.96). (a), (b), and (c) have the same meaning as in the left panel. The black, red, and green symbols represent XIS 0, 1, and 3 data, respectively. The average flux during the observation $F_{20-100\,keV} \sim 0.5 \times 10^{-9}$ erg cm^{-2} s^{-1}.

(A color version of this figure is available in the online journal.)

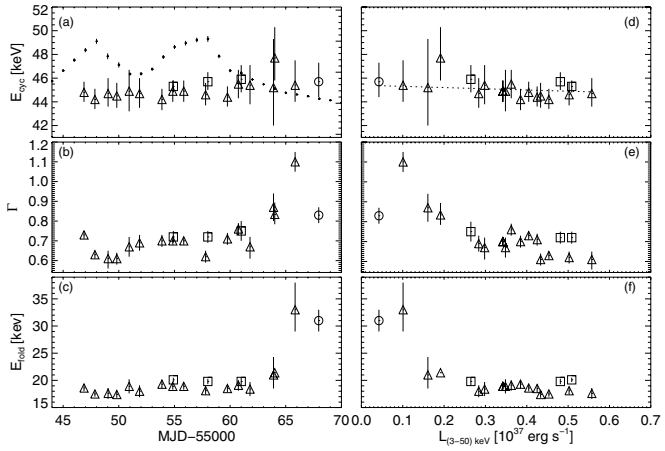

Figure 4. Left: evolution of the cyclotron line centroid energy $E_{\rm cyc}$ (a), photon index Γ (b), and folding energy $E_{\rm fold}$ (c) with time. In panel (a), the crosses represent the *Swift*-BAT light curve in arbitrary units. Right: evolution of $E_{\rm cyc}$ (d), Γ (e), and $E_{\rm fold}$ (f) with the (3–50) keV X-ray luminosity. The *RXTE*, *INTEGRAL*, and *Suzaku* observations are represented with triangles, squares, and a circle, respectively. In panel (d), the dashed line represents a linear fit to the data. Error bars are at 90% confidence.

the HXD, we fixed the constant to $c_{\rm GSO} = 0.88$ (the value obtained before adding the cyclotron line to the model), because when unconstrained, the best fit results in an unrealistic value of $c_{\rm GSO} = 0.4 \pm 0.1$. By doing this, the folding energy decreases from $E_{\rm fold} = 44^{+9}_{-6}$ to 31 ± 2 keV, while the power-law index and the cyclotron line energy remain constant within the errors. As seen in the middle and bottom panels of Figure 4, the photon index significantly decreases with increasing luminosity. The folding energy remains constant during the main part of the outburst, down to a luminosity of $L_{(3-50)\,\rm keV} \sim 0.26 \times 10^{37}$erg s^{-1}, and shows an increase in the last observations of the outburst. Both the folding energy and the photon index increase with decreasing luminosities. The values plotted in Figure 4 have been obtained leaving these two parameters free in the spectral fits. The increase of the photon index with decreasing X-ray luminosity indicates a softening of the spectrum, while the increase of the folding energy with decreasing X-ray luminosity indicates a hardening of the spectrum. In order to check if the spectrum becomes softer or harder as the luminosity decreases, in the last three *RXTE* observations, we fixed the folding energy to the mean value of the first 13 observations, $E_{\rm fold} = 18.4$ keV. By doing this, a slope of $(-0.44 \pm 0.04)/10^{37}$erg s^{-1} is obtained from a linear fit to the Γ versus $L_{\rm X}$ values, with a Pearson correlation coefficient of 0.82. This result indicates a softening of the spectrum with decreasing luminosity.

4. DISCUSSION

We have presented the first observations of a double-peaked outburst of A 0535+26 with *RXTE*, *INTEGRAL*, and *Suzaku*. The double-peaked outburst was the precursor of a giant one in 2009 December. Two double-peaked outbursts were also observed before a giant one in 1994 (Finger et al. 1996), while other giant outbursts do not show any precursor outbursts (Tueller et al. 2005). Another outburst with a peculiar shape (two separate peaks) was observed two orbital phases after the 2009 giant outburst (see Camero-Arranz et al. 2012).

We measured a pulse period of $P = 103.51263 \pm 0.00004$ s and spin-up of $\dot{P} = (-0.459 \pm 0.005) \times 10^{-8}$ s s^{-1} at MJD 55047.4, and a spin-up of $\dot{P} = (-1.104 \pm 0.002) \times 10^{-8}$ s s^{-1} at MJD 55056.87. These results are in agreement with the values obtained with *Fermi* Gamma-Ray Burst Monitor (GBM) by Camero-Arranz et al. (2012), who also present the long-term pulse period history of A 0535+26. We note that the changes in the spin-up rate along the outburst could be due to the outdated orbital solution. A new orbital solution is required to explore the pulse period evolution in more detail. A spin-up during normal outbursts has also been observed in the past (Caballero et al. 2008), providing evidence for an accretion disk around the neutron star during normal outbursts. The energy and luminosity dependent pulse profiles are remarkably stable compared to past observations of the source (see, e.g., Caballero et al. 2007; Naik et al. 2008), and consistent with those obtained with *Fermi*-GBM by Camero-Arranz et al. (2012) during the same period.

We observe no significant variation of the cyclotron line energy with the X-ray luminosity during the double-peaked outburst, and a significant decrease of the photon index Γ (spectral hardening) with increasing luminosity. A similar behavior has been observed in other outbursts of the source (e.g., Caballero et al. 2008; Müller et al. 2012a). In accreting X-ray pulsars, a positive or negative correlation of $E_{\rm cyc}$ with $L_{\rm X}$ is related to different accretion regimes. Following the theoretical predictions from Becker et al. (2012), the critical luminosity for A 0535+26 corresponds to $L_{\rm crit} \sim 6.78 \times 10^{37}$ erg s^{-1}. The observations presented here are well below that limit, with $L_{(3-50)\,\rm keV}$ ranging between ∼0.04 and ∼0.56 × 10^{37} erg s^{-1}, and therefore A 0535+26 is probably accreting in the sub-critical regime during the outburst. A positive correlation between $E_{\rm cyc}$ and $L_{\rm X}$ is expected for sub-critical sources. The fact that no correlation is observed might be due to the fact that our observations are near or below the Coulomb stopping limit, $L_{\rm coul}$, where little variation of $E_{\rm cyc}$ with $L_{\rm X}$ is expected (see Becker et al. 2012, for further details).

The double-peaked shape of the light curve could be due to perturbations in the Be disk around the optical companion. Moritani et al. (2011) showed that A 0535+26 exhibited strong Hα variability during, before, and after the giant outburst in 2009, and suggested that strong perturbations in the Be disk started about one cycle before the giant outburst. In addition, the Hα EW and *V*-band brightness showed an anticorrelation before the 2009 giant outburst (Yan et al. 2012; Camero-Arranz et al. 2012). This indicates that a mass ejection event took place before the giant outburst, producing a low-density region in the inner part of the disk that could explain the double-peaked profile (Yan et al. 2012). Interestingly, Yan et al. (2012) reported a similar Hα EW and *V*-band brightness evolution before the 1994 outburst, when two double-peaked outbursts took place before the giant one (Finger et al. 1996). Such an anticorrelation was not observed before the 2005 giant outburst, which took place without precursor outbursts. Double-peaked light curves have recently been observed in other sources, for instance GX 304−1 (Nakajima et al. 2012) and XTE J 1946+274 (Müller et al. 2012). While the spectral shape again remained relatively constant over the outburst for the latter, this is a special case, since two outbursts per orbit are observed. In the case of GX 304−1, the double-peaked outburst took place before a giant one, similar to what has been observed for A 0535+26, suggesting that double-peaked outbursts could be indicators of upcoming giant outbursts (Nakajima et al. 2012). The double-peaked outburst in the case of GX 304−1 was similar to that of A 0535+26 in terms of duration, lasting about 40 days. While in the case of A 0535+26 the two peaks reached a similar flux level, in the case of GX 304−1 the

second peak reached a flux two times higher than the first one. The intensities of the two peaks were $F_{(15-50)\,\mathrm{keV}} = (0.098 \pm 0.004)$ counts s^{-1} cm^{-2} (∼445 mCrab) at MJD 56075 and $F_{(15-50)\,\mathrm{keV}} = (0.196 \pm 0.008)$ counts s^{-1} cm^{-2} (∼891 mCrab) at MJD 56087, with a flux between the two peaks that dropped down to $F_{(15-50)\,\mathrm{keV}} = (0.021 \pm 0.001)$ counts s^{-1} cm^{-2} (∼95 mCrab) at MJD 56082. Note that the distances of the two sources are rather similar, with GX 304−1 being at ∼2.4 kpc (Parkes et al. 1980). The giant outburst of GX 304−1 lasted about 50 days, showing a first weaker peak that reached an X-ray flux of $F_{(15-50)\,\mathrm{keV}} = (0.163 \pm 0.007)$ counts s^{-1} cm^{-2} (∼741 mCrab) at MJD 56208. The flux then dropped down to zero (formally $F_{(15-50)\,\mathrm{keV}} = (0.004 \pm 0.021)$ counts s^{-1} cm^{-2} at MJD 56223), and increased again, reaching $F_{(15-50)\,\mathrm{keV}} = (0.406 \pm 0.015)$ counts s^{-1} cm^{-2} (∼1.85 Crab) at MJD 56234. Further simultaneous X-ray and optical observations of double-peaked outbursts are needed to better understand their origin and relation to giant ones.

We thank the anonymous referee for useful comments, the *RXTE*, *INTEGRAL*, and *Suzaku* teams for the scheduling of the observations, and ISSI (Bern) for their hospitality during our collaboration meetings. I.C. thanks Philippe Laurent for the help with the *INTEGRAL* analysis, Yuuki Moritani for useful discussions, and acknowledges financial support from the French Space Agency CNES through CNRS. K.P. and D.M.M. acknowledge support from NASA guest observer grants NNXIOAJ47G for *INTEGRAL* cycle 6 and NNXIOAJ48G for *Suzaku* cycle 4. J.W. and I.K. acknowledge partial funding from the Deutsches Zentrum für Luft- und Raumfahrt under contract number 50 OR 1113. A.C.-A. is supported by the grants AYA2009-07391 and SGR2009-811, as well as the Formosa program TW2010005 and iLINK program 2011-0303.

REFERENCES

Basko, M. M., & Sunyaev, R. A. 1976, MNRAS, 175, 395
Becker, P. A., Klochkov, D., Schönherr, G., et al. 2012, A&A, 544, A123
Bradt, H. V., Rothschild, R. E., & Swank, J. H. 1993, A&AS, 97, 355
Caballero, I. 2009, PhD thesis, IAAT Univ. Tuebingen
Caballero, I., Kretschmar, P., Pottschmidt, K., et al. 2009, ATel, 2337
Caballero, I., Kretschmar, P., Santangelo, A., et al. 2007, A&A, 465, L21
Caballero, I., Santangelo, A., Kretschmar, P., et al. 2008, A&A, 480, L17
Camero-Arranz, A., Finger, M. H., Wilson-Hodge, C. A., et al. 2012, ApJ, 754, 20
DeCesar, M. E., Boyd, P. T., Pottschmidt, K., et al. 2013, ApJ, 762, 61
Finger, M. H., Camero-Arranz, A., Kretschmar, P., Wilson, C., & Patel, S. 2006, BAAS, 38, 359
Finger, M. H., Wilson, R. B., & Harmon, B. A. 1996, ApJ, 459, 288
Jahoda, K., Swank, J. H., Giles, A. B., et al. 1996, Proc. SPIE, 2808, 59
Klochkov, D., Doroshenko, V., Santangelo, A., et al. 2012, A&A, 542, L28
Klochkov, D., Staubert, R., Santangelo, A., Rothschild, R. E., & Ferrigno, C. 2011, A&A, 532, A126
Koyama, K., Tsunemi, H., Dotani, T., et al. 2007, PASJ, 59, 23
Lund, N., Budtz-Jørgensen, C., Westergaard, N. J., et al. 2003, A&A, 411, L231
Moritani, Y., Nogami, D., Okazaki, A. T., et al. 2011, PASJ, 63, L25
Mowlavi, N., Kreykenbohm, I., Shaw, S. E., et al. 2006, A&A, 451, 187
Müller, D., et al. 2012a, A&A, submitted
Müller, S., Ferrigno, C., Kühnel, M., et al. 2012b, A&A, in press (arXiv:1211.6298)
Müller, S., Kühnel, M., Caballero, I., et al. 2012, A&A, 546, A125
Naik, S., Dotani, T., Terada, Y., et al. 2008, ApJ, 672, 516
Nakajima, M., Higa, M., Tsuboi, Y., et al. 2012, ATel, 4420
Nakajima, M., Mihara, T., Makishima, K., & Niko, H. 2006, ApJ, 646, 1125
Nowak, M. A., Hanke, M., Trowbridge, S. N., et al. 2011, ApJ, 728, 13
Parkes, G. E., Murdin, P. G., & Mason, K. O. 1980, MNRAS, 190, 537
Postnov, K., Staubert, R., Santangelo, A., Klochkov, D., Kretschmar, P., & Caballero, I. 2008, A&A, 480, L21
Rosenberg, F. D., Eyles, C. J., Skinner, G. K., & Willmore, A. P. 1975, Natur, 256, 628
Rothschild, R. E., Blanco, P. R., Gruber, D. E., et al. 1998, ApJ, 496, 538
Rothschild, R. E., Wilms, J., Tomsick, J., et al. 2006, ApJ, 641, 801
Rothschild, R. E., et al. 2013, ApJ, submitted
Schönherr, G., Wilms, J., Kretschmar, P., et al. 2007, A&A, 472, 353
Staubert, R., Klochkov, D., & Wilms, J. 2009, A&A, 500, 883
Staubert, R., Shakura, N. I., Postnov, K., et al. 2007, A&A, 465, L25
Steele, I. A., Negueruela, I., Coe, M. J., & Roche, P. 1998, MNRAS, 297, L5
Takahashi, T., Abe, K., Endo, M., et al. 2007, PASJ, 59, 35
Tanaka, Y. 1986, in IAU Colloq. 89, Radiation Hydrodynamics in Stars and Compact Objects, ed. D. Mihalas & K.-H. A. Winkler (Lecture Notes in Physics, Vol. 255; Dordrecht: Springer-Verlag), 198
Terada, Y., Mihara, T., Nakajima, M., et al. 2006, ApJL, 648, L139
Tsygankov, S. S., Lutovinov, A. A., Churazov, E. M., & Sunyaev, R. A. 2006, MNRAS, 371, 19
Tueller, J., Ajello, M., Barthelmy, S., et al. 2005, ATel, 504
Ubertini, P., Lebrun, F., Di Cocco, G., et al. 2003, A&A, 411, L131
Vedrenne, G., Roques, J.-P., Schönfelder, V., et al. 2003, A&A, 411, L63
Verner, D. A., Ferland, G. J., Korista, K. T., & Yakovlev, D. G. 1996, ApJ, 465, 487
White, N. E., Swank, J. H., & Holt, S. S. 1983, ApJ, 270, 711
Wilms, J., Allen, A., & McCray, R. 2000, ApJ, 542, 914
Yan, J., Li, H., & Liu, Q. 2012, ApJ, 744, 37